

---

# AN IMPROVED OPTIMAL PROXIMAL GRADIENT ALGORITHM FOR NON-BLIND IMAGE DEBLURRING

---

**Qingsong Wang**

School of Mathematics and Computational Science  
Xiangtan University  
Hunan, China 411105  
nothing2wang@hotmail.com

**Shengze Xu**

Department of Mathematics  
The Chinese University of Hong Kong  
Shatin, Hong Kong  
szxu@math.cuhk.edu.hk

**Xiaojiao Tong**

School of Mathematics and Computational Science  
Xiangtan University  
Hunan, China 411105  
dysfxtxj@hnfnu.edu.cn

**Tieyong Zeng\***

Department of Mathematics  
The Chinese University of Hong Kong  
Shatin, Hong Kong  
zeng@math.cuhk.edu.hk

## ABSTRACT

Image deblurring remains a central research area within image processing, critical for its role in enhancing image quality and facilitating clearer visual representations across diverse applications. This paper tackles the optimization problem of image deblurring, assuming a known blurring kernel. We introduce an improved optimal proximal gradient algorithm (IOptISTA), which builds upon the optimal gradient method and a weighting matrix, to efficiently address the non-blind image deblurring problem. Based on two regularization cases, namely the  $l_1$  norm and total variation norm, we perform numerical experiments to assess the performance of our proposed algorithm. The results indicate that our algorithm yields enhanced PSNR and SSIM values, as well as a reduced tolerance, compared to existing methods.

**Keywords:** Non-blind image deblurring, Optimal gradient method, Proximal gradient algorithm, Weighted matrix.

## 1 Introduction

Image deblurring, a critical process for restoring clarity to images obscured by factors such as motion blur or defocus, extends its utility across a multitude of domains, including image/video processing [36, 33, 18], signal processing [34, 25, 29, 11], traffic monitoring [2, 32, 28], and remote sensing [35, 19, 20]. Typically, image deblurring can be formulated as a linear inverse problem [7, 3], that is,

$$b = Ax + \varepsilon, \quad (1)$$

where  $A \in \mathbb{R}^{m \times n}$  represents the blur kernel,  $b \in \mathbb{R}^m$  is observed the blurred image,  $\varepsilon$  accounts for noise. However, solving this inverse problem to recover the original image is often fraught with challenges due to its ill-conditioned nature, which can result in non-unique solutions. To mitigate this, we formulate an optimization problem:

$$\min_{x \in \mathbb{R}^n} f(x) + h(x), \quad (2)$$

where  $f(x) := \frac{1}{2} \|Ax - b\|^2$ ,  $h(x)$  is the regularization component, which addresses the ill-posed nature of the problem by imposing specific properties or constraints on the solution  $x$ , such as  $l_1$  norm [27], total variation (TV) norm [24]. In this paper, we only consider the convex case for simplicity.

---

\*Corresponding author. Email: zeng@math.cuhk.edu.hk

Over the years, a multitude of algorithms has been developed to address the non-blind deblurring problem. Broadly, deblurring methods can be categorized into optimization-based approaches [5, 22] and deep learning techniques [23, 4, 12]. In this paper, we focus exclusively on optimization-based methods, which provide a structured framework for solving the convex optimization formulation of the problem. One of the most prominent algorithms in this category is the iterative shrinkage-thresholding algorithm (ISTA) [10], which is also known as the proximal gradient algorithm and is defined as follows:

$$x_{k+1} = \text{Prox}_{\frac{1}{L}h}\left(x_k - \frac{1}{L}\nabla f(x_k)\right), \quad (3)$$

where  $1/L > 0$  is the step size,  $L$  is the gradient Lipschitz constant of function  $f$ , and  $\text{Prox}_{\eta h}(\cdot)$  is the proximal operator which is defined as  $\text{Prox}_{\eta h}(x) := \operatorname{argmin}_{y \in \mathbb{R}^d} h(y) + \frac{1}{2\eta}\|y - x\|^2$ . The convergence of the ISTA is relatively slow, achieving a rate of  $\mathcal{O}(\frac{1}{k})$ . To address this issue, Beck et al. [6] introduced a modified version of ISTA called the fast iterative shrinkage thresholding algorithm (FISTA), namely the accelerated proximal gradient algorithm, which is defined as:

$$\begin{aligned} x_{k+1} &= \text{Prox}_{\frac{1}{L}h}\left(y_k - \frac{1}{L}\nabla f(y_k)\right), \\ \alpha_{k+1} &= \frac{1 + \sqrt{1 + 4\alpha_k^2}}{2}, \\ y_{k+1} &= x_k + \frac{\alpha_k - 1}{\alpha_{k+1}}(x_k - x_{k-1}), \end{aligned} \quad (4)$$

where  $\alpha_1 = 1$ , and FISTA achieves a faster convergence rate of  $\mathcal{O}(\frac{1}{k^2})$ . Based on the proximal gradient framework, the optimized gradient method (OGM) [15] can also be applied to solve the optimization problem (2) as:

$$\begin{aligned} y_{k+1} &= \text{Prox}_{\eta h}\left(x_k - \frac{1}{L}\nabla f(x_k)\right), \\ x_{k+1} &= y_{k+1} + \frac{\alpha_k - 1}{\alpha_{k+1}}(y_{k+1} - y_k) + \frac{\alpha_k}{\alpha_{k+1}}(y_{k+1} - x_k). \end{aligned} \quad (5)$$

We denote this algorithm as the proximal optimized gradient method (POGM). We know the term  $\frac{\alpha_k - 1}{\alpha_{k+1}}(y_{k+1} - y_k)$  can be viewed as the momentum term, while  $\frac{\alpha_k}{\alpha_{k+1}}(y_{k+1} - x_k)$  is called the correction term. However, the convergence of this algorithm is unclear now. Recently, to improve the convergence rate of the FISTA algorithm, Jang et al. [13] proposed the optimal iterative shrinkage thresholding algorithm (OptISTA), which is defined as:

$$\begin{aligned} y_{k+1} &= \text{Prox}_{\gamma_k \frac{1}{L}h}\left(y_k - \gamma_k \frac{1}{L}\nabla f(x_k)\right), \\ z_{k+1} &= x_k + \frac{1}{\gamma_k}(y_{k+1} - y_k), \\ x_{k+1} &= z_{k+1} + \frac{\alpha_k - 1}{\alpha_{k+1}}(z_{k+1} - z_k) + \frac{\alpha_k}{\alpha_{k+1}}(z_{k+1} - x_k), \end{aligned} \quad (6)$$

where  $\gamma_k > 0$ . It improves the leading convergence rate of FISTA by a factor of 2 in the  $\mathcal{O}(\frac{1}{k^2})$  term, although their analysis method is quite complex. When  $h(x) = 0$ , the OptISTA algorithm simplifies to the optimized gradient method (OGM) [15]. However, the OptISTA algorithm was only analyzed theoretically, and the efficiency of the algorithm was not verified through any numerical experiments. Other accelerated algorithms, such as FPGM2 [26] and APIRL1-AM [1], can also be employed to solve the optimization problem (2).

Alternatively, to further enhance the convergence speed of FISTA, Zulfiqar et al. [8] introduced the improved FISTA algorithm (IFISTA). IFISTA accelerates the optimization process by advancing the least-squares gradient descent by  $n$  steps, formulated as:  $x_{k+1} = \text{Prox}_{\frac{1}{L}h}\left(y_k - \frac{1}{L}W_n\nabla f(y_k)\right)$  in (4), where the weighting matrix is given by:

$$W_n := \sum_{i=1}^n \binom{n}{i} (-1)^{i-1} \left(\frac{1}{L}A^T A\right)^{i-1}. \quad (7)$$

Based on this framework, Wang et al. [30] proposed the IFISTA beyond Nesterov's momentum (IFISTA-BN) method to accelerate IFISTA by using a series of over-relaxation parameters instead of using the momentum term. Note that IFISTA and IFISTA-BN's effectiveness was primarily demonstrated in scenarios with low additive white Gaussian

noise. To address this limitation, Kumar and Sahoo [16] proposed the enhanced FISTA (EFISTA) algorithm, which achieves a similar convergence rate.

From the details of the algorithms mentioned above, we observe that the use of momentum techniques or weighting matrix can significantly accelerate convergence and enhance numerical performance. Furthermore, the optimized gradient method (OGM) achieves a faster convergence rate than the Nesterov acceleration method.

In this paper, we introduce two innovative algorithms that integrate the weighting matrix technique within the OGM framework to tackle the optimization problem (2). Specifically,

- **Well-defined Efficient Algorithm:** To expedite the algorithm's flexibility and convergence, we propose an improved optimal proximal gradient algorithm (referred to as Algorithm 1) designed to address the convex optimization problem (2) effectively.
- **Superior Performance in Non-blind Image Deblurring:** Leveraging the  $l_1$  norm and total variation (TV) norm, we demonstrate the numerical efficacy of our proposed algorithms on non-blind image deblurring tasks. Our methods consistently outperform existing algorithms in terms of numerical results.

The structure of the subsequent sections of this paper is as follows: Section 2 delineates the intricacies of the proposed algorithm (Algorithm 1). Section 3 showcases experimental outcomes on real-world datasets, thereby highlighting the superior performance of the proposed algorithm across two distinct regularization paradigms. Finally, Section 4 encapsulates our conclusions and proposes avenues for future research.

## 2 Algorithm

In this section, we develop an efficient algorithm to address the convex optimization problem (2), aiming to achieve superior numerical performance. A natural approach is to incorporate the weighting matrix  $W_n$  from (7) into the proximal gradient descent step as shown in (6), i.e.,

$$y_{k+1} = \text{Prox}_{\gamma_k \eta_k h}(y_k - \gamma_k \eta_k W_n \nabla f(x_k)), \quad (8)$$

which is equivalent to:

$$y_{k+1} = \underset{y}{\text{argmin}} h(y) + \langle y - y_k, \nabla f(x_k) \rangle + \frac{1}{2\gamma_k \eta_k} \|y - y_k\|_{W_n^{-1}}^2, \quad (9)$$

where  $\|x\|_{W_n}^2 = x^T W_n x$ . As far as we know, the OptISTA algorithm [13] was only analyzed theoretically, and the efficiency of the algorithm was not verified through any numerical experiments. This paper should be the first attempt, and it is combined with the weighting matrix technique to solve practical problems, such as the non-blind image deblurring task (2).

Based on this modification, we propose the following improved OptISTA (IOptISTA) algorithm. See Figure 1 for an illustration of the differences and connections between the OptISTA and IOptISTA algorithms.

---

**Algorithm 1 IOptISTA:** An improved OptISTA.

---

**Input:**  $b, A, \{\eta_k\}_{k \geq 0} \in (0, \lambda_{\max}^{-1}(A^T A)], \{\alpha_k\}_{k \geq 0} > 0$  and  $\{\gamma_k\}_{k \geq 0} > 0$ .

**Initialization:**  $W_n \succ 0, x_0 = y_0$ .

- 1: **while** stopping criteria is not met **do**
- 2:    $y_{k+1} = \text{Prox}_{\gamma_k \eta_k h}(y_k - \gamma_k \eta_k W_n \nabla f(x_k))$ .
- 3:    $z_{k+1} = x_k + \frac{1}{\gamma_k}(y_{k+1} - y_k)$ .
- 4:    $x_{k+1} = z_{k+1} + \frac{\alpha_k - 1}{\alpha_{k+1}}(z_{k+1} - z_k) + \frac{\alpha_k}{\alpha_{k+1}}(z_{k+1} - x_k)$ .
- 5:    $k = k + 1$ .
- 6: **end while**

**Output:**  $x_k$

---

In addition, we also given the setting of  $\alpha_k$  and  $\gamma_k$  from [13] in Algorithms 1 as following,

$$\alpha_k = \begin{cases} 1, & \text{if } k = 0, \\ \frac{1 + \sqrt{1 + 4\alpha_{k-1}^2}}{2}, & \text{if } 1 \leq k \leq K - 1, \\ \frac{1 + \sqrt{1 + 8\alpha_{K-1}^2}}{2}, & \text{if } k = K, \end{cases} \quad (10)$$

where  $K$  is the maximum number of iterations in Algorithm 1, and

$$\gamma_k = \frac{2\alpha_k}{\alpha_K^2}(\alpha_K^2 - 2\alpha_k^2 + \alpha_k), \quad k = 0, 1, \dots, K - 1. \quad (11)$$

We know that  $\gamma_k$  in Algorithm 1 depends on  $\alpha_K$ , thus the total iteration count  $K$  must be chosen before the start of the method. In practice, we select the maximum number of iterations  $K$ , compute the sequences  $\{\alpha_k\}$  and  $\{\gamma_k\}$ , and then iterate the algorithm. These two steps are not nested but sequential. Generally speaking, the calculation time will hardly increase because other algorithms, such as FISTA and MFISTA, also need time to calculate related parameters. There are many ways to select the step size  $\eta_k$ , such as constant step size, BB step size, adaptive step size, etc. However, this paper studies the non-blind deblurring optimization problem, that is, the operator  $A$  in (2) is known. We can directly compute the parameter  $L$  of the  $L$ -smooth function  $f$ . We set  $\eta_k = 1/L$  in the numerical part (Section 3) for simplicity. One advantage of the IOptISTA algorithm is that it is more convenient to use in practice.

Figure 1 demonstrates that the IOptISTA framework (Algorithm 1) offers greater flexibility and possibly achieves better acceleration than the OptISTA algorithm [13].

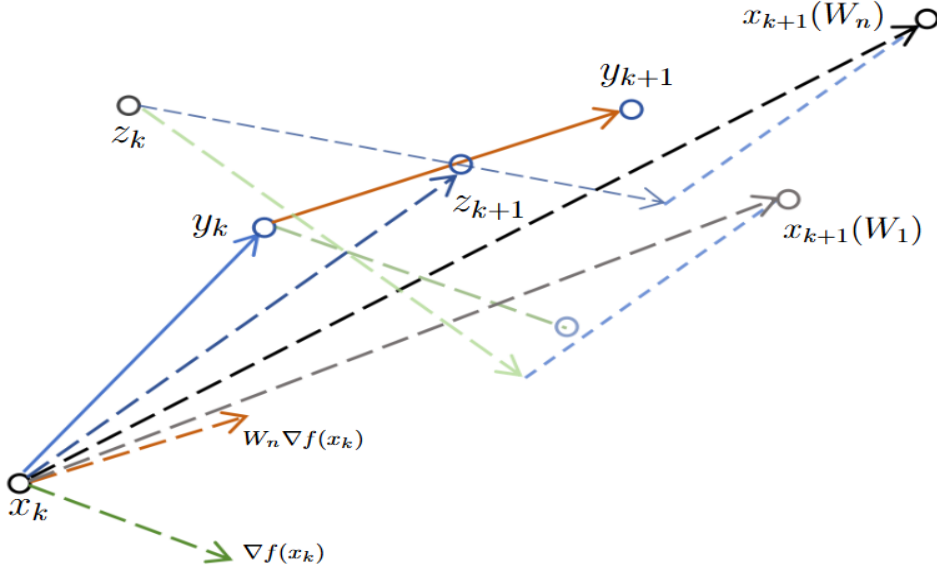


Figure 1: The illustration of the IOptISTA and OptISTA algorithms. Where “ $x_{k+1}(W_1)$ ” is the output of OptISTA, “ $x_{k+1}(W_n)$ ” is the output of IOptISTA.

**Remark 1.** From the IOptISTA framework in Algorithm 1, we have the following observations.

- When  $W_n = W_1 = I$  (identity matrix), the IOptISTA algorithm simplifies to the OptISTA algorithm [13].
- When  $W_n = I$  and  $h = 0$  in Algorithm 1, it reduces to the optimized gradient method (OGM) [15].

The convergence analysis of the IOptISTA algorithm (Algorithm 1) is beyond the scope of this paper, and we leave it as one of the future research topics. It is worth noting that through our experiments, we have found that the proposed algorithm is consistently convergent and can almost always achieve superior numerical results.

**Remark 2.** To ensure the convergence of the algorithm, a viable approach is to incorporate the monotonicity of the objective function ( $\phi(x) := f(x) + h(x)$ ) into the IOptISTA algorithm. For instance, for the 4-th step in the IOptISTA algorithm (Algorithm 1), we propose the following modification:

$$\hat{x}_{k+1} = z_{k+1} + \frac{\alpha_k - 1}{\alpha_{k+1}}(z_{k+1} - z_k) + \frac{\alpha_k}{\alpha_{k+1}}(z_{k+1} - x_k), \quad (12)$$

If  $\phi(\hat{x}_{k+1}) < \phi(x_k)$  then  $x_{k+1} = \hat{x}_{k+1}$  else  $x_{k+1} = x_k$ .

We denote this modification based on Algorithm 1 as the MOptISTA algorithm. In this way, we can always ensure the algorithm converges, meaning that the objective function  $\phi(x_k)$  forms a descending sequence. However, our experiments have revealed that the iteration time for the modified algorithm increases, and the numerical results

are slightly inferior to those obtained with Algorithm 1. See Figure 2 for details. We can see from Figure 2 that compared with the MOptISTA algorithm, Algorithm 1 can obtain better results in terms of error, PNSR, and SSIM values. Consequently, for the sake of simplicity, we opt to utilize Algorithm 1 in this paper.

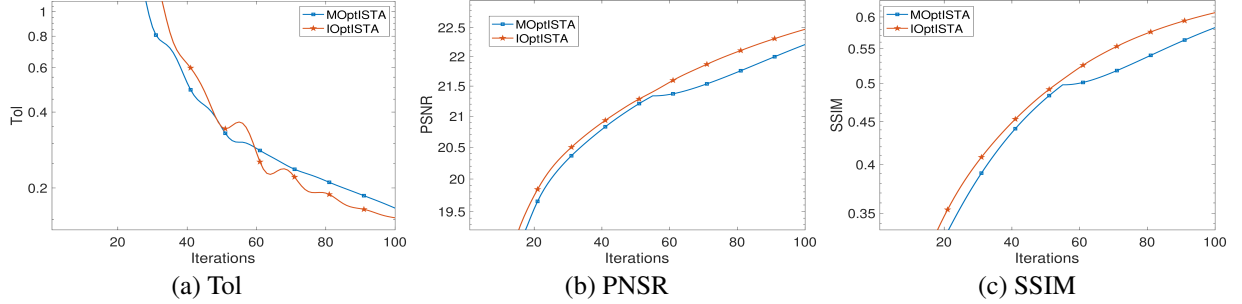


Figure 2: The numerical results for Figure 3(a) with “ $k = \text{fspecial}(\text{'disk'}, 13)$ ” and  $\varepsilon \sim \mathcal{N}(0, 10^{-3})$ .

In addition, we establish the following property of the IOptISTA algorithm.

**Lemma 1.** In Algorithm 1, we have  $x_K = y_K$ .

*Proof.* The proof of this lemma is detailed in A. □

Based on Lemma 1, we define the output of Algorithm 1 as  $x_k$ , rather than  $y_k$ , which is the convention in other acceleration algorithm frameworks, such as FISTA [6], IFISTA [8], and EFISTA [16].

### 3 Numerical experiments

In this section, we conduct a numerical study to evaluate the performance of the proposed algorithm under various regularization settings for non-blind image deblurring tasks. Furthermore, we compare the performance of our algorithm (Algorithm 1) with several well-established methods, including ISTA [10], IISTA (Improved ISTA), FISTA [6], EFITSA [16], and OptISTA [13]. We do not compare with the IFISTA algorithm [8] because it is a special case of the EFISTA algorithm [16]. The numerical experiments are implemented using MATLAB R2019a and executed on a computer equipped with an Intel CORE i7-14700KF @ 3.40GHz processor and 64GB of RAM.

The algorithm terminates under one of the following three conditions:

- (1) The maximum run time ( $T$ ) is reached.
- (2) The maximum number of iterations ( $K$ ) is reached.
- (3) All compared algorithms terminate when the tolerance level is satisfied:

$$\text{Tol} := \frac{1}{2} \|Ax - b\|^2 \leq 10^{-4}. \quad (13)$$

To quantitatively assess the quality of the restored images, we utilize the peak signal-to-noise ratio (PSNR)<sup>2</sup> and the structural similarity index (SSIM)<sup>3</sup> [31].

We utilize six images to demonstrate the numerical performance of the proposed algorithms, as depicted in Figure 3.

In addition, we use the commands “disk” and “gaussian” in MATLAB to blur the image, i.e., “ $s = \text{fspecial}(\text{'disk'}, a)$ ” or “ $s = \text{fspecial}(\text{'gaussian'}, b, c)$ ” with positive constants  $a, b, c > 0$ , and then processed with “ $\text{imfilter}(\text{im}, s, \text{'circular'})$ ” to produce blurred images.

In this section, we consider two regularization cases for  $h(x)$ : the  $l_1$  norm [27] and the total variation (TV) norm [24].

<sup>2</sup>PSNR =  $20 \log_{10} \left( \frac{255^2}{\text{MSE}} \right)$ , where  $\text{MSE} = \|\hat{x} - x\|^2$ ,  $\hat{x}$  and  $x$  are the restored and original images, respectively.

<sup>3</sup>SSIM =  $\frac{(2u_{\hat{x}}u_x + c_1)(2\sigma_{\hat{x}x} + c_2)}{(u_{\hat{x}}^2 + u_x^2 + c_1)(\sigma_{\hat{x}}^2 + \sigma_x^2 + c_2)}$ , where all parameters are defined as in [31].

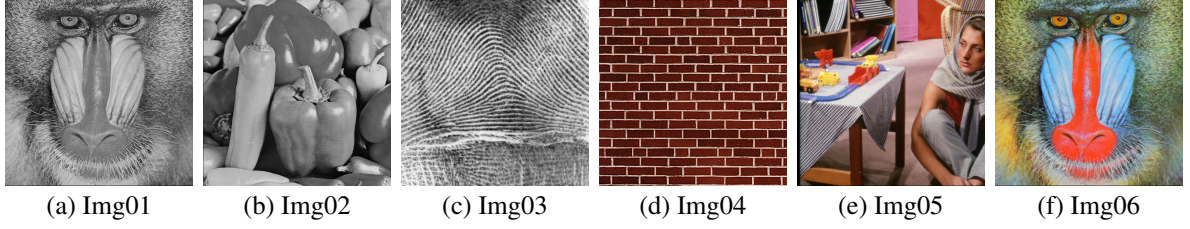


Figure 3: Details of the test images.

### 3.1 Setting of $n$ in $W_n$

In this subsection, we utilize Figure 3(a) and (d) to assess the numerical performance of  $W_n$  (as defined in (7)) under various values of  $n$  within Algorithm 1. For the sake of simplicity, we focus on the scenario where  $h = \lambda\|x\|_1$  with  $\lambda = 0.0001$ . Across all compared algorithms, the parameters are configured as  $T = 20$  seconds,  $K = 300$  iterations, and the initial iteration point is set to zero.

Subsequently, for this deblurring model, we employ Gaussian noise and disk blur algorithms for validation. Specifically, for Gaussian noise, we examine two cases:  $\varepsilon \sim \mathcal{N}(0, 10^{-4})$  and  $\varepsilon \sim \mathcal{N}(0, 5 \times 10^{-4})$ . Regarding the blur kernel, we consider different levels of blurring. For the selection of  $n$  in  $W_n$ , we explore 7 scenarios, namely  $n = \{2, 4, 6, 8, 10, 12, 14\}$ .

To demonstrate the enhancement achieved by incorporating  $W_n$  in IOptISTA (Algorithm 1), we also contrast it with the OptISTA algorithm, which corresponds to the case of  $W_n = W_1 = I$  in Algorithm 1. Refer to Table 1 for the outcomes. Additionally, we provide a detailed view of the last two columns in Table 1, as shown in Figure 4.

Table 1: The numerical results for the optimization problem (2) with  $h(x) = \lambda\|x\|_1$  for disk blurring kernel, and different  $n$  in  $W_n$  and noises.

Algorithm	Images	Img01				Img04			
	Noises	$\varepsilon \sim \mathcal{N}(0, 10^{-4})$		$\varepsilon \sim \mathcal{N}(0, 5 \times 10^{-4})$		$\varepsilon \sim \mathcal{N}(0, 10^{-4})$		$\varepsilon \sim \mathcal{N}(0, 5 \times 10^{-4})$	
	Kernels	12	14.5	12	13.5	7	12	7	11
OptISTA	Tol	6.3e-2	5.5e-2	8.8e-2	8.4e-2	1.3e-1	1.6e-1	1.4	1.7e-1
	PSNR	22.60	22.28	22.57	22.38	22.11	18.76	22.09	18.75
	SSIM	0.6227	0.5901	0.6190	0.6018	0.6679	0.5738	0.6670	0.5726
IOptISTA, $n = 2$	Tol	3.2e-2	2.9e-2	5.5e-2	5.3e-2	4.4e-2	4.6e-2	5.4e-2	5.9e-2
	PSNR	23.44	23.11	23.37	23.17	24.14	20.65	24.05	20.60
	SSIM	0.6938	0.6660	0.6829	0.6684	0.7378	0.6419	0.7342	0.6388
IOptISTA, $n = 4$	Tol	1.6e-2	1.5e-2	3.6e-2	3.6e-2	1.7e-2	1.5e-2	2.5e-2	2.6e-2
	PSNR	24.46	24.14	24.20	23.94	26.14	22.18	25.79	22.01
	SSIM	0.7593	0.7369	0.7305	0.7164	0.7995	0.6935	0.7884	0.6850
IOptISTA, $n = 6$	Tol	1.0e-2	9.5e-3	2.8e-2	2.8e-2	8.2e-3	8.8e-3	1.5e-2	1.9e-2
	PSNR	25.13	24.83	24.62	<b>24.21</b>	27.20	22.89	26.51	22.56
	SSIM	0.7927	0.7743	0.7448	<b>0.7291</b>	0.8296	0.7168	0.8096	0.7016
IOptISTA, $n = 8$	Tol	7.4e-3	7.5e-3	2.4e-2	2.5e-2	6.5e-3	6.1e-3	1.3e-2	1.5e-2
	PSNR	25.62	25.34	24.83	<b>24.21</b>	27.79	23.33	26.74	22.81
	SSIM	0.8139	0.7973	0.7475	0.7286	0.8447	0.7311	0.8163	0.7086
IOptISTA, $n = 10$	Tol	5.9e-3	6.7e-3	2.1e-2	2.3e-2	5.6e-3	5.1e-3	1.1e-2	1.3e-2
	PSNR	26.03	25.72	<b>24.91</b>	24.06	28.24	23.64	26.83	22.92
	SSIM	0.8284	0.8130	<b>0.7442</b>	0.7224	0.8548	0.7438	0.8186	0.7132
IOptISTA, $n = 12$	Tol	4.8e-3	<b>7.0e-3</b>	1.9e-2	2.1e-2	4.7e-3	<b>4.1e-3</b>	1.0e-2	<b>1.2e-2</b>
	PSNR	26.36	<b>26.00</b>	24.90	23.83	28.65	<b>23.89</b>	26.88	<b>22.96</b>
	SSIM	0.8392	<b>0.8284</b>	0.7383	0.7136	0.8632	<b>0.7539</b>	0.8196	<b>0.7154</b>
IOptISTA, $n = 14$	Tol	<b>4.0e-3</b>	1.6e+31	<b>1.6e-2</b>	<b>2.0e-2</b>	<b>3.7e-3</b>	2.5e+19	<b>8.6e-3</b>	2.5e+19
	PSNR	<b>26.64</b>	< 0	24.84	23.58	<b>29.05</b>	< 0	<b>26.91</b>	< 0
	SSIM	<b>0.8475</b>	< 0	0.7311	0.7039	<b>0.8719</b>	< 0	<b>0.8208</b>	< 0

By comparing Table 1 and Figure 4, we can discern the following observations:

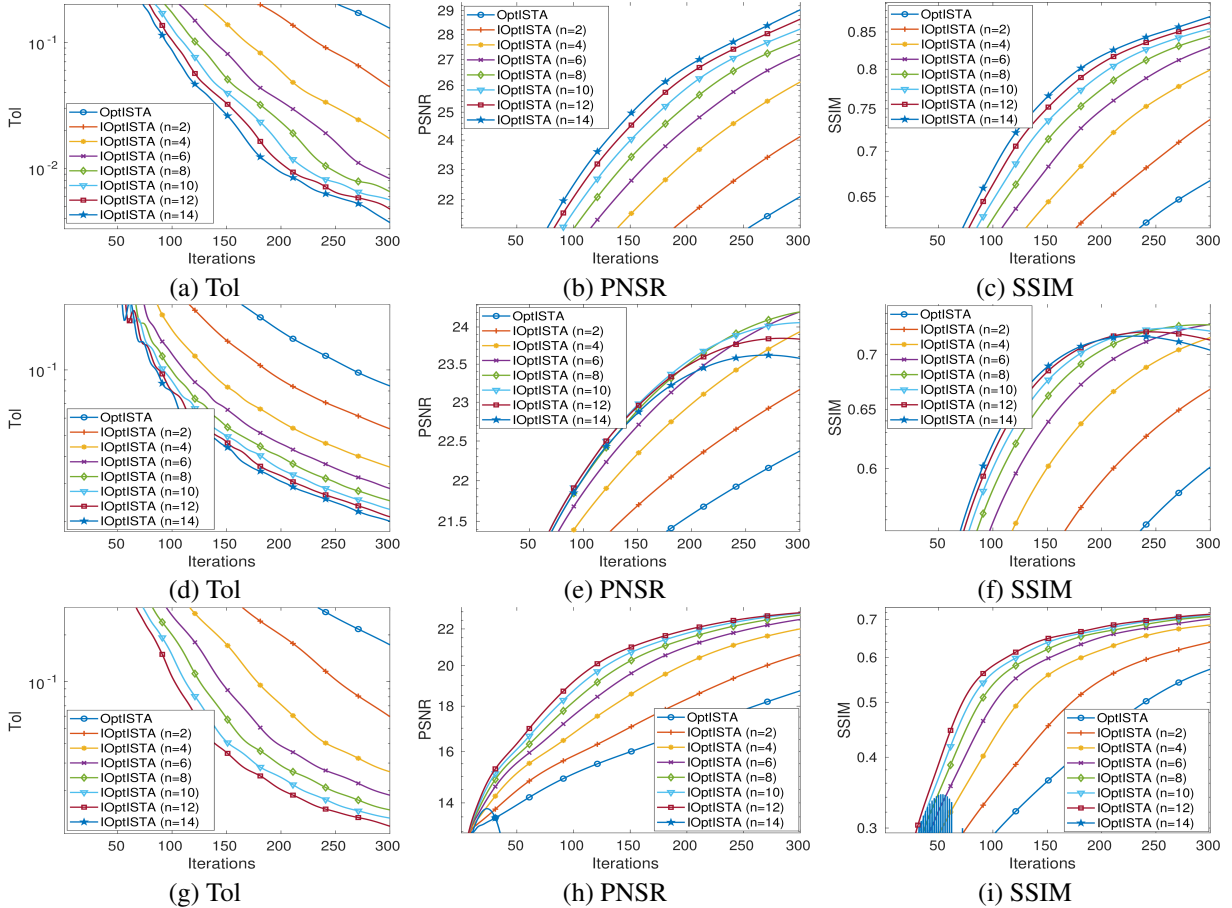


Figure 4: The Tol, PSNR and SSIM results for different images, noises and  $n$  in  $W_n$ . First row: Figure 3(d) with “ $k = \text{fspecial}(\text{'disk'}, 7)$ ” and  $\varepsilon \sim \mathcal{N}(0, 1e - 4)$ . Second row: Figure 3(a) with “ $k = \text{fspecial}(\text{'disk'}, 13.5)$ ” and  $\varepsilon \sim \mathcal{N}(0, 5e - 4)$ . Third row: Figure 3(d) with “ $k = \text{fspecial}(\text{'disk'}, 11)$ ” and  $\varepsilon \sim \mathcal{N}(0, 5e - 4)$ .

- When the noise variance and blur degree are relatively low, a larger  $n$  in  $W_n$  yields lower error and superior PSNR and SSIM values for the proposed algorithm.
- Under a constant noise variance, as the blur level increases, increasing  $n$  within a certain range leads to improved numerical results. However, beyond a certain threshold, an excessive value of  $n$  in  $W_n$  can degrade the results or even cause the algorithm to diverge and fail.
- If the blur degree is held constant, a similar numerical effect is observed as the noise variance increases.

Through numerical experiments, we have determined that a larger  $n$  in  $W_n$  of Algorithm 1 does not automatically result in better numerical performance. This relationship is dependent on both the noise variance and the degree of blur.

We observed that the impact of increasing  $n$  on the algorithm’s numerical performance is not straightforward; it is influenced by the variance of the noise, the degree of blur and the step size of the proposed algorithm. When  $n = 14$ , one of the main reasons for the algorithm divergence should be that the step size is too large. In summary, under fixed step size, for scenarios with low noise variance and mild blur, selecting a relatively large  $n$  can further enhance the algorithm’s numerical performance. Conversely, for cases with higher noise variance or more severe blur, a smaller  $n$  is preferred to ensure algorithm stability, even if it does not yield the best numerical results. Nonetheless, all selections of  $W_n$  lead to improved performance compared to algorithms without the use of  $W_n$ .

For example, algorithms such as IEFISTA [8], IEFISTA-BN [30], and EFISTA [16], which have convergence theoretical guarantees, will also diverge in numerical experiments when  $n$  is large and the step size is not changed, just like the last case in Table 1.

The numerical disparity between employing  $W_n$  and not employing it within an algorithm remains significantly large, thus warranting further exploration into the selection methodology for  $n$  as part of our future research endeavours. For simplicity, we fixed  $n = 12$  in  $W_n$  for all compared algorithms in the following numerical experiments.

### 3.2 Case one: $l_1$ norm regularization

In this subsection, we focus on the case where  $h(x) = \lambda\|x\|_1$  [27, 21] in the optimization problem (2), which is formulated as:

$$\min_{x \in \mathbb{R}^n} \frac{1}{2} \|Ax - b\|^2 + \lambda \|x\|_1, \quad (14)$$

where  $\lambda > 0$  is a constant parameter, and  $\|x\|_1 := \sum_{i=1}^n |x_i|$ . We set  $\lambda = 0.0001$  to evaluate the performance of all compared algorithms. For these algorithms, the parameters are configured with  $T = 20$  seconds,  $K = 300$  iterations, and the initial iteration point is set to zero.

We employ six images within the optimization problem (14) to assess the numerical performance of the proposed algorithms under various blurred kernels and noise conditions. The results are compiled in Table 2.

The results presented in Table 2 demonstrate that, when compared to other algorithms, the IOptISTA consistently attains the lowest error values. Across all experiments, the IOptISTA algorithm outperforms other methods in delivering superior PSNR and SSIM values. Collectively, the proposed algorithm exhibits enhanced numerical performance. For further insights, refer to Figures 5 and 6.

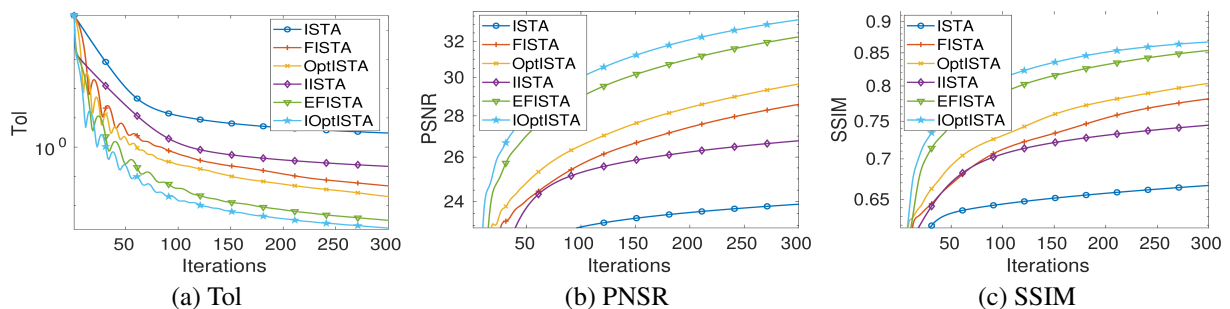


Figure 5: The Tol, PSNR and SSIM results for Figure 3(b) with “ $k = \text{fspecial}(\text{'disk'}, 12)$ ” and  $\varepsilon \sim \mathcal{N}(0, 1e - 4)$ .

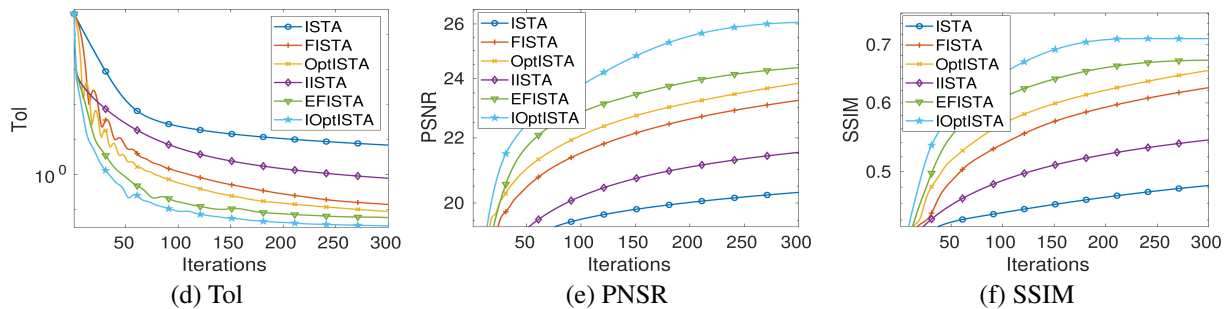


Figure 6: The Tol, PSNR and SSIM results for Figure 3(e) with “ $k = \text{fspecial}(\text{'gaussian'}, 25, 35)$ ” and  $\varepsilon \sim \mathcal{N}(0, 5e - 4)$ .

Figures 5 and 6 illustrate the trends in error (Tol), PSNR, and SSIM values across iterations for Figure 3(b) with “ $k = \text{fspecial}(\text{'disk'}, 12)$ ” and  $\varepsilon \sim \mathcal{N}(0, 1e - 4)$ , and for the Figure 3(e) with “ $k = \text{fspecial}(\text{'gaussian'}, 25, 35)$ ” and  $\varepsilon \sim \mathcal{N}(0, 5e - 4)$ , respectively. These figures indicate that from the initial stages, the IOptISTA algorithm outperforms other methods. Notably, IOptISTA achieves superior results in terms of both error, PSNR, and SSIM values. We can also observe that when the blur operator is fixed, the performance of all algorithms degrades as the noise level increases, and the numerical performance gap between the algorithms becomes smaller. Nonetheless, the algorithm proposed in this paper consistently achieves better numerical results.

In Figures 7 and 8, we present the blurred and restored images resulting from the compared algorithms. As can be observed, the numerical outcomes of the IOptISTA algorithm are markedly superior.

Table 2: The numerical results for the optimization problem (14) with different blurred kernels and noises under six compared algorithms.

Algorithm	Images	Img01		Img02		Img03		Img04		Img05		Img06	
	Kernels	12.5	(24,40)	12	(24,40)	13	(20,30)	8	(15,30)	9	(25,35)	8	(10,23)
Noise $\varepsilon \sim \mathcal{N}(0, 10^{-4})$													
ISTA	Tol	2.6e0	2.3e0	3.0e0	3.0e0	7.9e0	8.9e0	1.4e+1	2.2e+1	6.8e0	6.9e0	6.5e-1	9.0e-1
	PSNR	19.70	19.64	23.89	23.56	16.43	16.61	14.93	15.79	21.29	20.31	21.57	22.40
	SSIM	0.2934	0.2906	0.6669	0.6609	0.1911	0.2221	0.2602	0.3784	0.5269	0.4821	0.3937	0.4644
FISTA	Tol	1.2e-1	7.9e-2	4.7e-2	4.4e-2	2.5e-1	3.0e-1	2.2e-1	1.8e-1	1.9e-1	1.0e-1	1.8e-2	1.7e-2
	PSNR	21.85	21.23	28.59	27.69	21.56	19.64	19.72	22.81	25.27	23.26	25.19	25.72
	SSIM	0.5458	0.4768	0.7816	0.7500	0.7466	0.6258	0.6152	0.6885	0.7362	0.6266	0.7200	0.7528
OptISTA	Tol	6.3e-2	4.2e-2	2.0e-2	2.1e-2	1.0e-1	1.3e-1	1.0e-1	5.1e-2	8.9e-2	5.3e-2	8.2e-3	8.5e-3
	PSNR	22.60	21.65	29.66	28.62	22.91	20.63	21.15	24.66	26.55	23.86	26.30	26.56
	SSIM	0.6223	0.5244	0.8040	0.7689	0.8152	0.7035	0.6616	0.7478	0.7846	0.6583	0.7827	0.7961
IISTA	Tol	4.0e-1	1.0e0	2.4e-1	1.1e0	1.6e0	1.0e0	1.1e0	8.6e-1	7.9e-1	7.4e-1	6.2e-2	6.7e-2
	PSNR	20.84	18.93	26.78	21.36	18.89	18.24	17.61	19.61	23.39	21.54	23.65	24.48
	SSIM	0.4255	0.3595	0.7447	0.5814	0.5342	0.4715	0.4960	0.5761	0.6513	0.5443	0.5956	0.6630
EFISTA	Tol	1.0e-2	9.3e-3	3.1e-3	4.5e-3	9.9e-3	1.6e-2	1.2e-2	6.0e-3	1.0e-2	9.2e-3	1.0e-3	1.1e-3
	PSNR	25.34	22.99	32.28	30.76	25.88	23.44	26.31	27.77	30.42	25.93	29.75	29.18
	SSIM	0.8003	0.6496	0.8539	0.8121	0.9106	0.8425	0.8023	0.8434	0.8778	0.7486	0.8950	0.8848
IOptISTA	Tol	<b>4.5e-3</b>	<b>6.2e-3</b>	<b>1.7e-3</b>	<b>3.8e-3</b>	<b>4.2e-3</b>	<b>7.1e-3</b>	<b>4.5e-3</b>	<b>2.7e-3</b>	<b>3.8e-3</b>	<b>4.9e-3</b>	<b>5.0e-4</b>	<b>5.0e-4</b>
	PSNR	<b>26.70</b>	<b>23.66</b>	<b>33.28</b>	<b>31.48</b>	<b>26.80</b>	<b>24.63</b>	<b>27.89</b>	<b>28.86</b>	<b>31.81</b>	<b>26.85</b>	<b>31.05</b>	<b>30.28</b>
	SSIM	<b>0.8467</b>	<b>0.6978</b>	<b>0.8671</b>	<b>0.8244</b>	<b>0.9285</b>	<b>0.8789</b>	<b>0.8412</b>	<b>0.8835</b>	<b>0.8973</b>	<b>0.7811</b>	<b>0.9164</b>	<b>0.9066</b>
Noise $\varepsilon \sim \mathcal{N}(0, 5 \times 10^{-4})$													
ISTA	Tol	2.6e0	2.3e0	3.1e0	3.1e0	7.9e0	8.9e0	1.4e+1	2.2e+1	6.9e0	6.9e0	6.5e-1	9.1e-1
	PSNR	19.70	19.64	23.89	23.56	16.43	16.61	14.93	15.79	21.29	20.31	21.57	22.40
	SSIM	0.2934	0.2906	0.6669	0.6609	0.1911	0.2221	0.2602	0.3784	0.5269	0.4821	0.3938	0.4644
FISTA	Tol	1.5e-1	1.1e-1	7.4e-2	7.2e-2	2.8e-1	3.3e-1	2.4e-1	1.9e-1	2.2e-1	1.4e-1	2.3e-2	2.3e-2
	PSNR	21.84	21.22	28.56	27.67	21.55	19.64	19.71	22.80	25.26	23.25	25.15	25.69
	SSIM	0.5445	0.4761	0.7780	0.7472	0.7460	0.6255	0.6147	0.6880	0.7340	0.6250	0.7167	0.7499
OptISTA	Tol	8.9e-2	6.9e-2	4.6e-2	4.8e-2	1.3e-1	1.6e-1	1.1e-1	6.5e-2	1.2e-1	8.8e-2	1.3e-2	1.3e-2
	PSNR	22.57	21.64	29.54	28.56	22.88	20.62	21.13	24.62	26.51	23.84	26.16	26.46
	SSIM	0.6182	0.5222	0.7932	0.7616	0.8136	0.7025	0.6605	0.7465	0.7783	0.6542	0.7732	0.7896
IISTA	Tol	4.1e-1	9.2e-1	2.5e-1	1.0e0	1.6e0	1.1e0	1.2e0	8.8e-1	8.3e-1	7.7e-1	6.9e-2	7.3e-2
	PSNR	20.84	19.04	26.77	21.36	18.89	18.24	17.61	19.61	23.39	21.54	23.64	24.47
	SSIM	0.4255	0.3614	0.7440	0.5811	0.5341	0.4715	0.4958	0.5761	0.6510	0.5441	0.5952	0.6623
EFISTA	Tol	4.6e-2	9.5e-2	3.9e-2	3.7e-2	5.1e-2	5.7e-2	3.0e-2	2.9e-2	5.1e-2	1.1e-1	9.4e-3	1.2e-2
	PSNR	24.74	22.37	30.48	29.36	24.27	23.25	25.69	27.17	29.21	24.39	27.65	27.96
	SSIM	0.7469	0.6179	0.7952	0.7589	0.8803	0.8320	0.7827	0.8237	0.8207	0.6722	0.8237	0.8374
IOptISTA	Tol	<b>1.8e-2</b>	<b>2.8e-2</b>	<b>1.6e-2</b>	<b>2.6e-2</b>	<b>1.9e-2</b>	<b>2.7e-2</b>	<b>1.0e-2</b>	<b>1.2e-2</b>	<b>1.9e-2</b>	<b>3.4e-2</b>	<b>2.4e-3</b>	<b>2.8e-3</b>
	PSNR	<b>24.99</b>	<b>23.17</b>	<b>30.67</b>	<b>29.82</b>	<b>25.34</b>	<b>24.03</b>	<b>26.21</b>	<b>27.26</b>	<b>29.40</b>	<b>26.06</b>	<b>27.83</b>	<b>28.30</b>
	SSIM	<b>0.7484</b>	<b>0.6429</b>	<b>0.8098</b>	<b>0.7674</b>	<b>0.8904</b>	<b>0.8529</b>	<b>0.7969</b>	<b>0.8332</b>	<b>0.8338</b>	<b>0.7115</b>	<b>0.8302</b>	<b>0.8453</b>

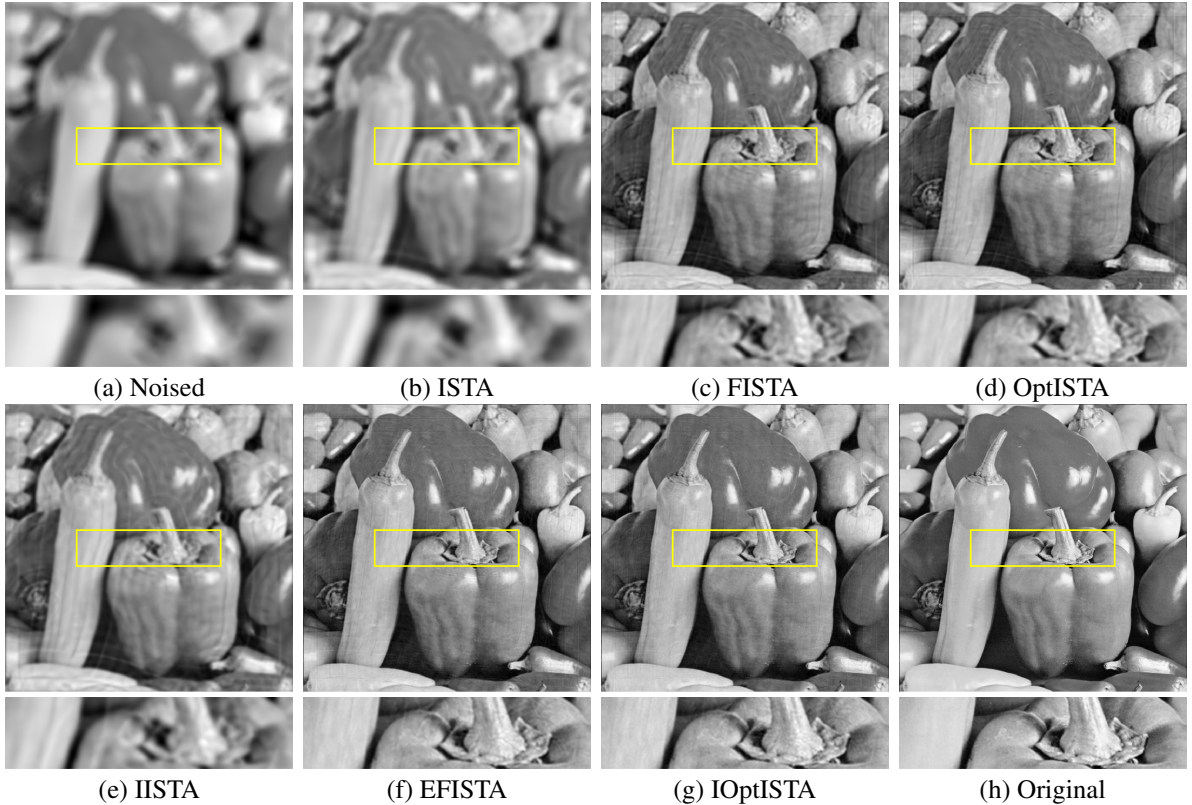


Figure 7: Blurred and restored images for the Figure 3(b) with “ $k = \text{fspecial}(\text{'disk'}, 12)$ ” and  $\varepsilon \sim \mathcal{N}(0, 1e - 4)$ .

### 3.3 Case two: Total variation (TV) regularization

In this subsection, we focus on the case where  $h(x) = \lambda \|x\|_{\text{TV}}$  [9, 14] in the optimization problem (2), which is formulated as:

$$\min_{x \in \mathbb{R}^n} \frac{1}{2} \|Ax - b\|^2 + \lambda \|x\|_{\text{TV}}, \quad (15)$$

where  $\lambda > 0$  and  $\|x\|_{\text{TV}} := \sum_{i=2}^n |x_i - x_{i-1}|$  represents the total variation (TV) norm of  $x$  [24]. To implement the proximal operator of the TV norm, we utilize the direct algorithm<sup>4</sup> from [17]. We set  $\lambda = 0.0001$  to assess the performance of all compared algorithms. For these algorithms, the parameters are configured with  $T = 20$  seconds,  $K = 200$  iterations, and the initial iteration point is zero.

We apply all images from Figure 3 to the optimization problem (15) to evaluate the performance of the proposed algorithms. Detailed numerical results are presented in Table 3.

The table further corroborates the conclusions drawn in Subsection 3.2: the IOptISTA algorithm consistently attains lower error rates under identical stopping conditions when compared to other methods. Additionally, IOptISTA typically achieves higher PSNR and SSIM values, see Figures 9 and 10 for details.

In summary, a comprehensive suite of numerical experiments has substantiated the effectiveness of the proposed algorithms. This paper establishes that integrating the weighting matrix technique with the optimal gradient method markedly enhances convergence and elevates numerical performance.

## 4 Conclusion and future works

This paper addressed the non-blind image deblurring problem by proposing an improved optimal proximal gradient algorithm for its solution. Specifically, we developed the IOptISTA and MOptISTA algorithms, whose superior convergence speed has been demonstrated through numerical experiments. These experiments, employing  $l_1$  norm and

<sup>4</sup><https://lcondat.github.io/software.html>

Table 3: The numerical results for the optimization problem (15) with different blurred kernels and noises under six compared algorithms.

Algorithm	Images	Img01		Img02		Img03		Img04		Img05		Img06	
	Kernels	12	(24,40)	12	(24,40)	13	(20,30)	7	(14,30)	8	(24,34)	7	(10,20)
Noise $\varepsilon \sim \mathcal{N}(0, 10^{-4})$													
ISTA	Tol	3.6e0	3.2e0	4.6e0	4.8e0	9.3e0	1.2e+1	1.6e+1	3.2e+1	1.1e+1	1.1e+1	9.1e-1	1.3e0
	PSNR	19.62	19.53	23.54	23.18	16.26	16.42	14.64	15.25	21.34	20.12	21.54	22.11
	SSIM	0.2854	0.2804	0.6573	0.6512	0.1660	0.1924	0.2221	0.3177	0.5302	0.4712	0.3858	0.4352
FISTA	Tol	2.9e-1	2.2e-1	1.2e-1	1.1e-1	8.5e-1	7.2e-1	9.4e-1	5.2e-1	5.0e-1	2.5e-1	6.0e-2	5.7e-2
	PSNR	21.02	20.63	27.53	26.75	19.71	18.55	18.05	21.82	23.89	22.62	24.00	24.59
	SSIM	0.4406	0.3968	0.7568	0.7336	0.5985	0.5088	0.4940	0.6543	0.6737	0.5939	0.6165	0.6655
OptISTA	Tol	2.0e-1	1.6e-1	6.0e-2	5.9e-2	3.6e-1	4.2e-1	5.1e-1	1.9e-1	2.8e-1	1.2e-1	4.5e-2	4.5e-2
	PSNR	21.32	20.85	28.58	27.63	20.82	19.19	19.35	23.91	24.67	23.10	24.43	24.91
	SSIM	0.4748	0.4203	0.7824	0.7540	0.6832	0.5726	0.5670	0.7298	0.7133	0.6194	0.6476	0.6889
IISTA	Tol	5.3e-1	1.7e0	3.6e-1	2.0e0	2.5e0	1.5e0	2.5e0	2.2e0	1.2e0	9.2e-1	1.1e-1	1.1e-1
	PSNR	20.66	18.63	26.25	20.60	18.18	17.90	16.87	19.20	23.05	21.84	23.42	24.10
	SSIM	0.3987	0.3371	0.7308	0.5788	0.4554	0.4248	0.4183	0.5560	0.6328	0.5566	0.5739	0.6290
EFISTA	Tol	4.3e-2	3.6e-2	8.8e-3	1.3e-2	3.6e-2	4.8e-2	4.4e-2	2.2e-2	3.8e-2	2.4e-2	8.5e-3	7.1e-3
	PSNR	22.98	21.91	31.22	29.81	24.04	21.79	24.27	26.89	27.83	24.36	26.86	26.87
	SSIM	0.6441	0.5393	0.8364	0.7997	0.8505	0.7634	0.7468	0.8208	0.8223	0.6886	0.8022	0.8068
IOptISTA	Tol	<b>2.4e-2</b>	<b>2.0e-2</b>	<b>4.8e-3</b>	<b>6.0e-2</b>	<b>1.6e-2</b>	<b>2.2e-2</b>	<b>1.7e-2</b>	<b>9.3e-3</b>	<b>1.7e-2</b>	<b>1.4e-2</b>	<b>4.4e-3</b>	<b>3.5e-3</b>
	PSNR	<b>23.80</b>	<b>22.38</b>	<b>32.23</b>	<b>30.88</b>	<b>25.24</b>	<b>22.86</b>	<b>26.35</b>	<b>27.89</b>	<b>29.34</b>	<b>24.98</b>	<b>28.03</b>	<b>27.75</b>
	SSIM	<b>0.7067</b>	<b>0.5869</b>	<b>0.8538</b>	<b>0.8210</b>	<b>0.8856</b>	<b>0.8118</b>	<b>0.8040</b>	<b>0.8447</b>	<b>0.8587</b>	<b>0.7183</b>	<b>0.8490</b>	<b>0.8429</b>
Noise $\varepsilon \sim \mathcal{N}(0, 10^{-3})$													
ISTA	Tol	3.8e0	3.4e0	4.7e0	4.9e0	9.5e0	1.2e+1	1.6e+1	3.2e+1	1.2e+1	1.1e+1	9.4e-1	1.3e0
	PSNR	19.62	19.53	23.54	23.18	16.26	16.42	14.64	15.25	21.34	20.12	21.54	22.11
	SSIM	0.2854	0.2803	0.6573	0.6512	0.1660	0.1923	0.2221	0.3177	0.5302	0.4712	0.3858	0.4352
FISTA	Tol	4.1e-1	3.5e-1	2.4e-1	2.3e-1	9.8e-1	8.4e-1	1.0e0	5.8e-1	6.5e-1	4.0e-1	8.7e-2	8.3e-2
	PSNR	21.01	20.62	27.50	26.73	19.71	18.55	18.04	21.81	23.88	22.61	23.98	24.56
	SSIM	0.4399	0.3958	0.7545	0.7311	0.5982	0.5085	0.4938	0.6537	0.6722	0.5921	0.6146	0.6636
OptISTA	Tol	3.2e-1	2.8e-1	1.8e-1	1.8e-1	4.8e-1	5.4e-1	5.7e-1	2.5e-1	4.3e-1	2.7e-1	7.1e-2	6.9e-2
	PSNR	21.31	20.84	28.52	27.57	20.80	19.18	19.34	23.87	24.65	23.09	24.39	24.86
	SSIM	0.4734	0.4184	0.7774	0.7481	0.6823	0.5717	0.5662	0.7281	0.7099	0.6160	0.6440	0.6854
IISTA	Tol	6.5e-1	1.8e0	4.9e-1	2.2e0	2.6e0	1.6e0	2.6e0	2.3e0	1.4e0	1.1e0	1.4e-1	1.3e-1
	PSNR	20.65	18.62	26.24	20.60	18.17	17.89	16.87	19.20	23.05	21.84	23.41	24.09
	SSIM	0.3984	0.3367	0.7298	0.5788	0.4553	0.4247	0.4182	0.5558	0.6322	0.5562	0.5728	0.6280
EFISTA	Tol	1.4e-1	1.5e-1	1.2e-1	1.3e-1	1.4e-1	1.5e-1	8.6e-2	7.5e-2	1.5e-1	1.7e-1	2.8e-2	2.6e-2
	PSNR	22.80	21.81	30.26	29.23	23.70	21.66	23.81	26.38	27.37	24.21	26.18	26.34
	SSIM	0.6246	0.5251	0.7880	0.7571	0.8364	0.7546	0.7300	0.8037	0.7863	0.6617	0.7663	0.7789
IOptISTA	Tol	<b>1.2e-1</b>	<b>1.3e-1</b>	<b>1.0e-2</b>	<b>1.2e-1</b>	<b>1.1e-1</b>	<b>1.2e-1</b>	<b>5.2e-2</b>	<b>5.8e-2</b>	<b>1.2e-1</b>	<b>1.5e-1</b>	<b>2.0e-2</b>	<b>2.0e-2</b>
	PSNR	<b>23.27</b>	<b>22.11</b>	<b>30.43</b>	<b>29.40</b>	<b>24.24</b>	<b>22.50</b>	<b>24.95</b>	<b>26.58</b>	<b>27.90</b>	<b>24.62</b>	<b>26.53</b>	<b>26.59</b>
	SSIM	<b>0.6572</b>	<b>0.5552</b>	<b>0.7912</b>	<b>0.7515</b>	<b>0.8528</b>	<b>0.7914</b>	<b>0.7646</b>	<b>0.8086</b>	<b>0.7916</b>	<b>0.6643</b>	<b>0.7830</b>	<b>0.7895</b>



Figure 8: Blurred and restored images for the Figure 3(e) with “ $k = \text{fspecial}(\text{'gaussian'}, 25, 35)$ ” and  $\varepsilon \sim \mathcal{N}(0, 5e-4)$ .

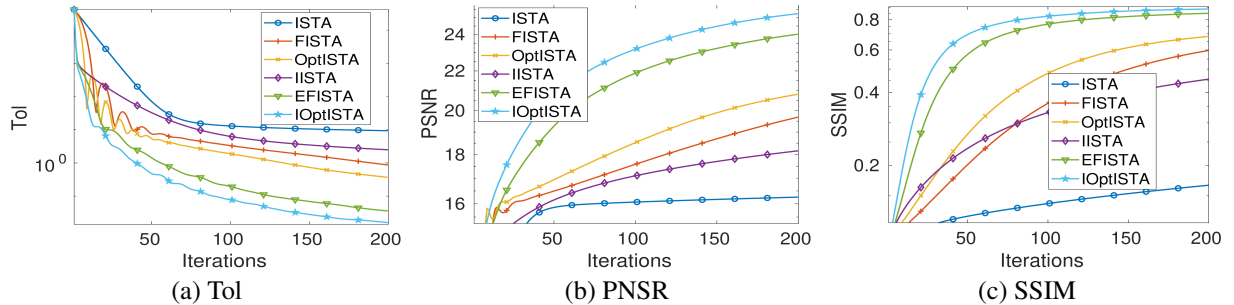


Figure 9: The Tol, PSNR and SSIM results for Figure 3(c) with “ $k = \text{fspecial}(\text{'disk'}, 13)$ ” and  $\varepsilon \sim \mathcal{N}(0, 1e-4)$ .

TV norm regularizations, confirmed the efficiency of our proposed methods, achieving lower error rates and higher PSNR and SSIM values compared to existing methods, thus showcasing their superior restoration performance.

In the future, we aim to conduct a comprehensive theoretical convergence analysis of the proposed algorithms to complement the experimental findings. Additionally, we plan to explore the application of these methods to nonconvex optimization problems in image and video deblurring, further extending their utility in computational imaging.

## Declarations

**Conflict of Interest:** On behalf of all authors, the corresponding author states that there is no conflict of interest.

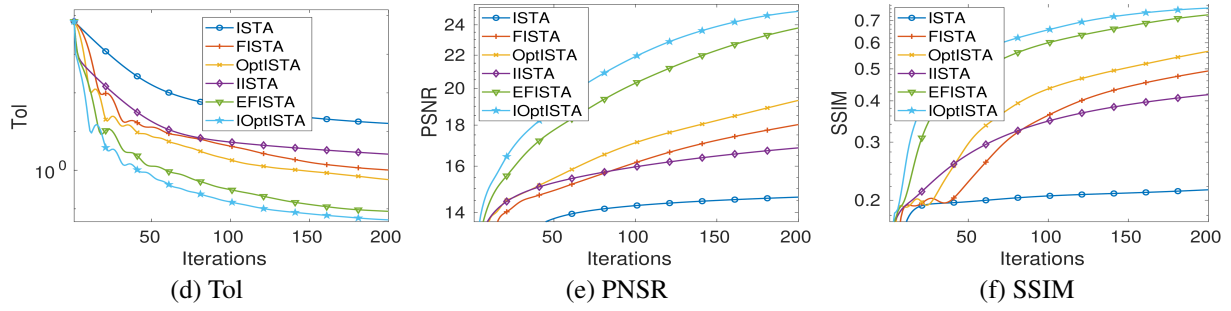


Figure 10: The Tol, PSNR and SSIM results for Figure 3(d) with “ $k = \text{fspecial}(\text{'disk'}, 7)$ ” and  $\varepsilon \sim \mathcal{N}(0, 1e - 3)$ .

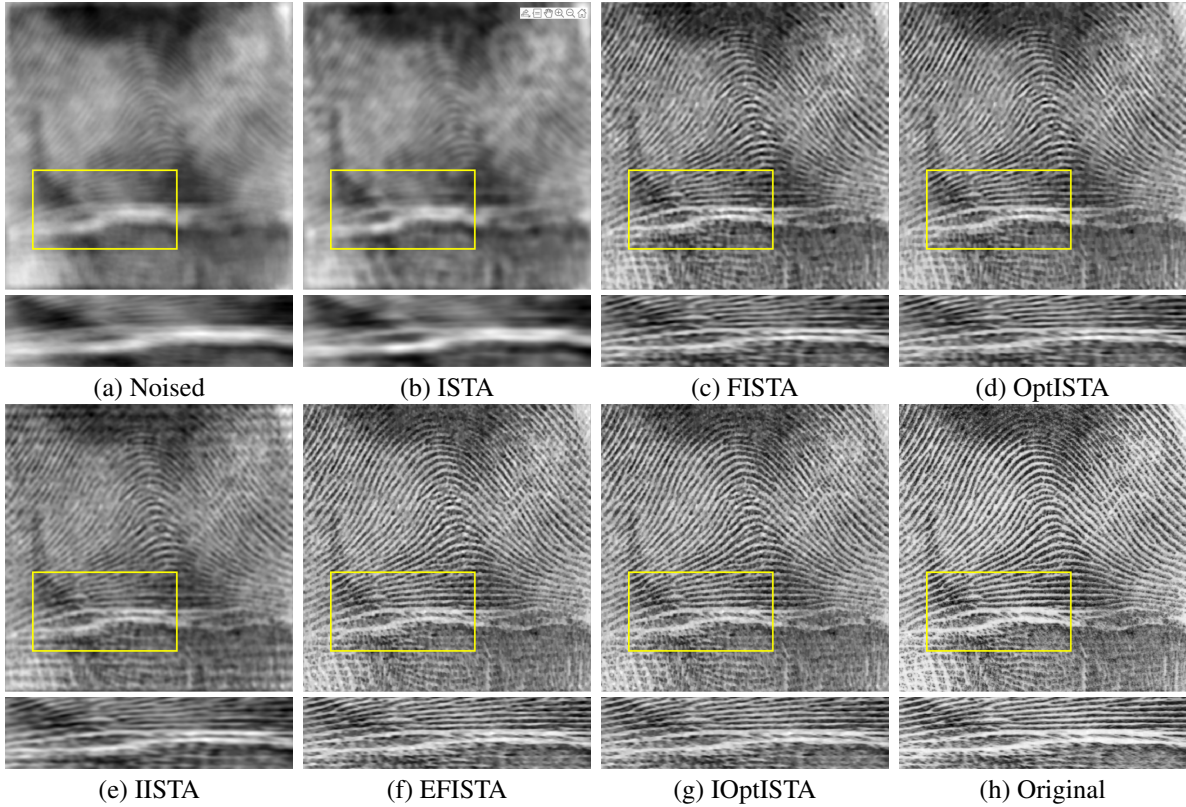


Figure 11: Blurred and restored images for the Figure 3(c) with “ $k = \text{fspecial}(\text{'disk'}, 13)$ ” and  $\varepsilon \sim \mathcal{N}(0, 1e - 4)$ .

**Funding:** This research is supported by the National Natural Science Foundation of China (NSFC) grant 12171145, 12331011, 12401415, 12471282.

**Data Availability Statement:** Data will be available upon reasonable request.

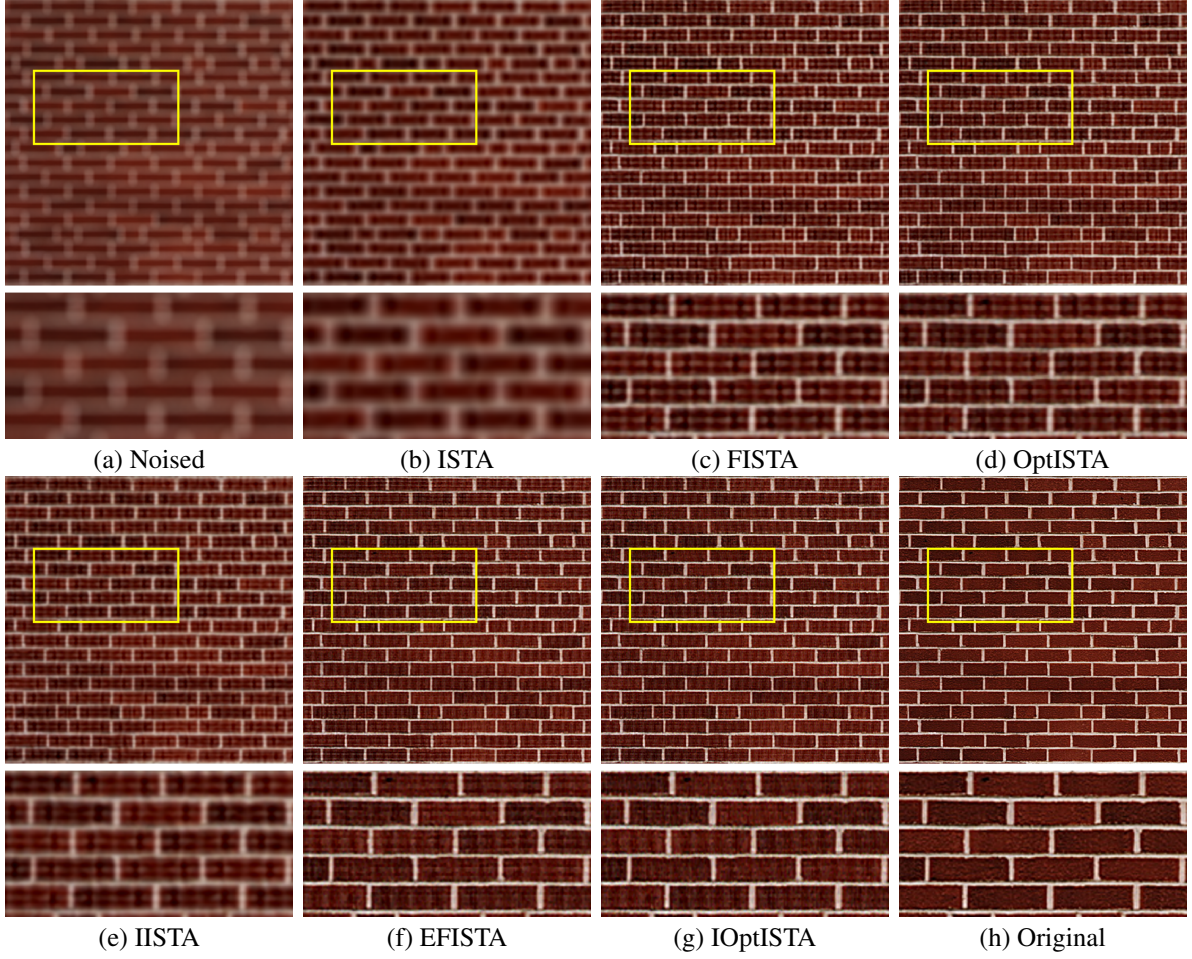


Figure 12: Blurred and restored images for the Figure 3(d) with “ $k = \text{fspecial}(\text{'disk'}, 7)$ ” and  $\varepsilon \sim \mathcal{N}(0, 1e - 3)$ .

## A Proof of Lemma 1

Before to prove Lemma 1, we need the following lemmas.

**Lemma 2.** (Lemma 16 in [13]) Let  $\{t_{i,j}\}_{i \in [1:K], j \in [0:K-1]}$  and  $\{s_{i,j}\}_{i \in [1:K], j \in [0:K-1]}$  be

$$t_{i+1,j} = \begin{cases} t_{j+1,j} + \sum_{k=j+1}^i \left( \frac{2\alpha_j}{\alpha_{k+1}} - \frac{1}{\alpha_{k+1}} t_{k,j} \right), & \text{if } j \in [0 : i - 1], \\ 1 + \frac{2\alpha_{i-1}}{\alpha_{i+1}}, & \text{if } j = i, \end{cases}$$

$$s_{i+1,j} = \begin{cases} t_{i+1,j} - t_{i,j}, & \text{if } j \in [0 : i - 1], \\ t_{i+1,j}, & \text{if } j = i. \end{cases}$$

Then,

$$t_{i+1,j} = \sum_{k=j+1}^{i+1} s_{k,j} \text{ for } j \in [0 : i] \text{ and } s_{i+1,j} = \begin{cases} \frac{\alpha_i - 1}{\alpha_{i+1}} s_{i,j}, & \text{if } j \in [0 : i - 2], \\ \frac{\alpha_i - 1}{\alpha_{i+1}} (s_{i,i-1} - 1), & \text{if } j = i - 1, \\ 1 + \frac{2\alpha_{i-1}}{\alpha_{i+1}}, & \text{if } j = i. \end{cases}$$

Now we convert  $x$  and  $y$ -iterates of IOptISTA (Algorithm 1) into the following form.

**Lemma 3.** Let

$$\gamma_i = \frac{2\alpha_i}{\alpha_K^2} (\alpha_K^2 - 2\alpha_i^2 + \alpha_i) \text{ for } i \in [0 : K - 1],$$

$$t_{i+1,j} = \begin{cases} t_{j+1,j} + \sum_{k=j+1}^i \left( \frac{2\alpha_j}{\alpha_{k+1}} - \frac{1}{\alpha_{k+1}} t_{k,j} \right), & \text{if } j \in [0 : i-1], \\ 1 + \frac{2\alpha_i-1}{\alpha_{i+1}}, & \text{if } j = i. \end{cases}$$

Denote  $h'(y_{j+1}) := \frac{1}{\eta_j \gamma_j} (y_j - \eta_j \gamma_j W_n \nabla f(x_j) - y_{j+1}) \in \partial h(y_{j+1})$ , then,  $\{x_1, \dots, x_K\}$  and  $\{y_1, \dots, y_K\}$  of the following form:

$$\begin{aligned} y_{i+1} &= x_0 - \sum_{j \in [0:i]} \gamma_j \eta_j W_n \nabla f(x_j) - \sum_{j \in [0:i]} \gamma_j \eta_j h'(y_{j+1}) \quad \text{for } i \in [0 : K-1], \\ x_{i+1} &= x_0 - \sum_{j \in [0:i]} t_{i+1,j} \eta_j W_n \nabla f(x_j) - \sum_{j \in [0:i]} t_{i+1,j} \eta_j h'(y_{j+1}) \quad \text{for } i \in [0 : K-1] \end{aligned} \quad (16)$$

is equal to  $x$ -iterates and  $y$ -iterates generated by Algorithm 1 respectively.

*Proof.* Denote  $\{\hat{x}_1, \dots, \hat{x}_K\}$  and  $\{\hat{y}_1, \dots, \hat{y}_K\}$  to be sequence generated by Algorithm 1, it shows that  $x_0 = y_0$  and  $\hat{y}_1 = y_1$ . We can get that

$$\hat{y}_1 = \text{Prox}_{\gamma_0 \eta_0 h}(y_0 - \gamma_0 \eta_0 W_n \nabla f(x_0)) = x_0 - \gamma_0 \eta_0 W_n \nabla f(x_0) - \gamma_0 \eta_0 h'(\hat{y}_1).$$

For  $x$ -iterate, we have

$$\begin{aligned} \hat{x}_1 &= x_1 + \frac{\alpha_0 - 1}{\alpha_1} (z_1 - z_0) + \frac{\alpha_0}{\alpha_1} (z_1 - z_0) \\ &= x_0 + \frac{1}{\gamma_0} (\hat{y}_1 - y_0) + \frac{1}{\alpha_1} (x_0 + \frac{1}{\gamma_0} (\hat{y}_1 - y_0) - x_0) \\ &= x_0 - \frac{1}{\gamma_0} \gamma_0 \eta_0 (W_n \nabla f(x_0) + h'(\hat{y}_1)) - \frac{1}{\alpha_1} \frac{1}{\gamma_0} \gamma_0 \eta_0 (W_n \nabla f(x_0) + h'(\hat{y}_1)) \\ &= x_0 - \eta_0 (1 + \frac{1}{\alpha_1}) W_n \nabla f(x_0) - \eta_0 (1 + \frac{1}{\alpha_1}) h'(\hat{y}_1) \\ &= x_0 - t_{1,0} \eta_0 W_n \nabla f(x_0) - t_{1,0} \eta_0 h'(\hat{y}_1) \\ &= x_1. \end{aligned}$$

Now we suppose  $x_k = \hat{x}_k$  and  $y_k = \hat{y}_k$  for  $1 \leq k \leq i$  and  $1 \leq i \leq K-1$ . Then we have  $\hat{y}_{i+1} = y_{i+1}$  from the uniqueness of the proximal operator, and

$$\begin{aligned} \hat{y}_{i+1} &= \text{Prox}_{\gamma_i \eta_i h}(\hat{y}_i - \gamma_i \eta_i W_n \nabla f(x_i)) \\ &= y_i - \gamma_i \eta_i W_n \nabla f(x_i) - \gamma_i \eta_i h'(\hat{y}_{i+1}) \\ &= x_0 - \sum_{j \in [0:i-1]} \gamma_j \eta_j W_n \nabla f(x_j) - \sum_{j \in [0:i-1]} \gamma_j \eta_j h'(y_{j+1}) - \gamma_i \eta_i W_n \nabla f(x_i) - \gamma_i \eta_i h'(\hat{y}_{i+1}) \\ &= x_0 - \sum_{j \in [0:i]} \gamma_j \eta_j W_n \nabla f(x_j) - \sum_{j \in [0:i]} \gamma_j \eta_j h'(y_{j+1}) \\ &= y_{i+1}. \end{aligned}$$

For  $x$ -iterate, it shows that

$$\begin{aligned} z_{i+1} &= x_0 - \sum_{j \in [0:i-1]} t_{i,j} \eta_j \nabla f(x_j) - \sum_{j \in [0:i-1]} t_{i,j} \eta_j h'(\hat{y}_{j+1}) - \frac{1}{\gamma_i} (\gamma_i \eta_i W_n \nabla f(x_i) + \gamma_i \eta_i h'(\hat{y}_{i+1})) \\ &= x_0 - \sum_{j \in [0:i-1]} t_{i,j} \eta_j W_n \nabla f(x_j) - \sum_{j \in [0:i-1]} t_{i,j} \eta_j h'(\hat{y}_{j+1}) - \eta_i W_n \nabla f(x_i) - \eta_i h'(\hat{y}_{i+1}). \end{aligned}$$

Based on the above equation, we have

$$\begin{aligned} \hat{x}_{i+1} &= z_{i+1} + \frac{\alpha_i - 1}{\alpha_{i+1}} (z_{i+1} - z_i) + \frac{\alpha_i}{\alpha_{i+1}} (z_{i+1} - \hat{x}_i) \\ &= x_0 - \sum_{j \in [0:i-1]} t_{i,j} \eta_j W_n \nabla f(x_j) - \sum_{j \in [0:i-1]} t_{i,j} \eta_j h'(y_{j+1}) - \eta_i W_n \nabla f(x_i) - \eta_i h'(y_{i+1}) \\ &\quad - \frac{\alpha_i - 1}{\alpha_{i+1}} \left( \sum_{j \in [0:i-2]} s_{i,j} \eta_j W_n \nabla f(x_j) + \sum_{j \in [0:i-2]} s_{i,j} \eta_j h'(y_{j+1}) \right) \end{aligned}$$

$$\begin{aligned}
& - \frac{\alpha_i - 1}{\alpha_{i+1}} ((t_{i,i-1} - 1)\eta_{i-1}W_n \nabla f(x_{i-1}) + (t_{i,i-1} - 1)\eta_{i-1}h'(y_i)) \\
& - \frac{\alpha_i - 1}{\alpha_{i+1}} (\eta_i W_n \nabla f(x_i) + \eta_i h'(y_{i+1})) - \frac{\alpha_i}{\alpha_{i+1}} (\eta_i W_n \nabla f(x_i) + \eta_i h'(y_{i+1})).
\end{aligned}$$

From Lemma 2, it shows that

$$\begin{aligned}
\frac{\alpha_i - 1}{\alpha_{i+1}} s_{i,j} &= s_{i+1,j} \quad \text{for } j \in [0 : i - 2], \\
\frac{\alpha_i - 1}{\alpha_{i+1}} (t_{i,i-1} - 1) &= s_{i+1,i-1}.
\end{aligned}$$

Thus, we have

$$\begin{aligned}
\hat{x}_{i+1} &= x_0 - \sum_{j \in [0:i-1]} t_{i,j} \eta_j W_n \nabla f(x_j) - \sum_{j \in [0:i-1]} t_{i,j} \eta_j h'(y_{j+1}) - \eta_i W_n \nabla f(x_i) - \eta_i h'(y_{i+1}) \\
& - \sum_{j \in [0:i-2]} s_{i+1,j} \eta_j W_n \nabla f(x_j) - \sum_{j \in [0:i-2]} s_{i+1,j} \eta_j h'(y_{j+1}) - s_{i+1,i-1} \eta_{i-1} W_n \nabla f(x_{i-1}) \\
& - s_{i+1,i-1} \eta_{i-1} h'(y_i) - \frac{\alpha_i - 1}{\alpha_{i+1}} (\eta_i W_n \nabla f(x_i) + \eta_i h'(y_{i+1})) \\
& - \frac{\alpha_i}{\alpha_{i+1}} (\eta_i W_n \nabla f(x_i) + \eta_i h'(y_{i+1})) \\
& = x_0 - \sum_{j \in [0:i-1]} t_{i+1,j} \eta_j W_n \nabla f(x_j) - \sum_{j \in [0:i-1]} t_{i+1,j} \eta_j h'(y_{j+1}) \\
& - \eta_i (1 + \frac{2\alpha_i - 1}{\alpha_{i+1}}) W_n \nabla f(x_i) - \eta_i (1 + \frac{2\alpha_i - 1}{\alpha_{i+1}}) h'(y_{i+1}) \\
& = x_0 - \sum_{j \in [0:i]} t_{i+1,j} \eta_j W_n \nabla f(x_j) - \sum_{j \in [0:i]} t_{i+1,j} \eta_j h'(y_{j+1}) \\
& = x_{i+1}.
\end{aligned}$$

Based on mathematical induction, we finish the proof.  $\square$

Now we are ready to prove Lemma 1.

*Proof.* From Lemma 18 in [13], it shows that

$$\frac{\alpha_{j+1}}{2\alpha_j - 1} (t_{K,j} - 1) - 1 = \frac{\alpha_{j+1} - 1}{2\alpha_{j+1} - 1} (t_{K,j+1} - 1).$$

Based on the above equation, we can get that the equation

$$\gamma_j = \frac{2\alpha_j}{\alpha_K^2} (\alpha_K^2 - 2\alpha_j^2 + \alpha_i) = t_{K,j}$$

holds for all  $j \in [0 : K - 1]$ . From (16) in Lemma 3 with  $i = K - 1$ , we have

$$\begin{aligned}
x_K &= x_0 - \sum_{j \in [0:K-1]} t_{K,j} \eta_j W_n \nabla f(x_j) - \sum_{j \in [0:K-1]} t_{K,j} \eta_j h'(y_{j+1}) \\
& = x_0 - \sum_{j \in [0:K-1]} \gamma_j \eta_j W_n \nabla f(x_j) - \sum_{j \in [0:K-1]} \gamma_j \eta_j h'(y_{j+1}) \\
& = y_K.
\end{aligned}$$

This completes the proof.  $\square$

## References

- [1] Tarmizi Adam, Alexander Malyshev, Mohd Fikree Hassan, Nur Syarafina Mohamed, and Md Sah Hj Salam. Accelerated proximal iterative re-weighted  $l_1$  alternating minimization for image deblurring. *arXiv:2309.05204*, 2023.
- [2] Sanaz Aliyan and Ali Broumandnia. A new machine learning approach to deblurring license plate using k-means clustering method. *International Journal of Advanced Research in Artificial Intelligence*, 1(2), 2012.
- [3] Simon R. Arridge, Peter Maass, Ozan Öktem, and Carola-Bibiane Schönlieb. Solving inverse problems using data-driven models. *Acta Numer.*, 28:1–174, 2019.
- [4] Trishna Barman and Bhabesh Deka. A deep learning-based joint image super-resolution and deblurring framework. *IEEE Trans. Artif. Intell.*, 5(6):3160–3173, 2024.
- [5] Amir Beck. *First-Order Methods in Optimization*. SIAM, 2017.
- [6] Amir Beck and Marc Teboulle. A fast iterative shrinkage-thresholding algorithm for linear inverse problems. *SIAM J. Imaging Sci.*, 2(1):183–202, 2009.
- [7] Martin Benning and Martin Burger. Modern regularization methods for inverse problems. *Acta Numer.*, 27:1–111, 2018.
- [8] Md. Zulfiquar Ali Bhotto, M. Omair Ahmad, and M. N. S. Swamy. An improved fast iterative shrinkage thresholding algorithm for image deblurring. *SIAM J. Imaging Sci.*, 8(3):1640–1657, 2015.
- [9] Raymond H. Chan, Tony F. Chan, and Chiu-Kwong Wong. Cosine transform based preconditioners for total variation deblurring. *IEEE Trans. Image Process.*, 8(10):1472–1478, 1999.
- [10] I. Daubechies, M. Defrise, and C. De Mol. An iterative thresholding algorithm for linear inverse problems with a sparsity constraint. *Communications on Pure and Applied Mathematics: A Journal Issued by the Courant Institute of Mathematical Sciences*, 57(11):1413–1457, 2004.
- [11] Amir Eqtetae and Alireza Ahmadyfard. Blind image deblurring using both L0 and L1 regularization of max-min prior. *Neurocomputing*, 592:127727, 2024.
- [12] Yuxiang Hui, Yang Liu, Yaofang Liu, Fan Jia, Jinshan Pan, Raymond H. Chan, and Tiejong Zeng. VJT: A video transformer on joint tasks of deblurring, low-light enhancement and denoising. *Arxiv: 2401.14754*, 2024.
- [13] Ujiyeong Jang, Shuvomoy Das Gupta, and Ernest K. Ryu. Computer-assisted design of accelerated composite optimization methods: OptISTA. *Arxiv: 2305.15704*, 2023.
- [14] Bowu Jiang and Wenkai Lu. Primal-dual optimization strategy with total variation regularization for prestack seismic image deblurring. *IEEE Trans. Geosci. Remote. Sens.*, 59(1):884–893, 2021.
- [15] Donghwan Kim and Jeffrey A. Fessler. Optimized first-order methods for smooth convex minimization. *Math. Program.*, 159(1-2):81–107, 2016.
- [16] Avinash Kumar and Sujit Kumar Sahoo. Enhanced FISTA for non-blind image deblurring. In *2024 International Conference on Signal Processing and Communications (SPCOM)*, pages 1–5, 2024.
- [17] Condat Laurent. A direct algorithm for 1D total variation denoising. *IEEE Signal Proc. Letters*, 20(11):1054–1057, 2013.
- [18] Chen Li, Li Song, Rong Xie, and Wenjun Zhang. L0 structure-prior assisted blur-intensity aware efficient video deblurring. *Neurocomputing*, 483:195–209, 2022.
- [19] Zhiyuan Li, Jie Li, Yueting Zhang, Jiayi Guo, and Yirong Wu. A noise-robust blind deblurring algorithm with wavelet-enhanced diffusion model for optical remote sensing images. *IEEE J. Sel. Top. Appl. Earth Obs. Remote. Sens.*, 17:16236–16254, 2024.
- [20] Mushui Liu, Yunlong Yu, Yingming Li, Zhong Ji, Wen Chen, and Yang Peng. Lightweight mimo-wnet for single image deblurring. *Neurocomputing*, 516:106–114, 2023.
- [21] Cheng Lu. *Efficient Algorithms for Markov Random Fields, Isotonic Regression, Graph Fused Lasso, and Image Segmentation*. PhD thesis, University of California, Berkeley, USA, 2017.
- [22] Yurii E. Nesterov. *Lectures on Convex Optimization*, volume 137 of *Springer Optimization and Its Applications*. Springer International Publishing, 2018.
- [23] Yuhui Quan, Peikang Lin, Yong Xu, Yuesong Nan, and Hui Ji. Nonblind image deblurring via deep learning in complex field. *IEEE Trans. Neural Networks Learn. Syst.*, 33(10):5387–5400, 2022.
- [24] L Rudin, S Osher, and E Fatemi. Nonlinear total variation based noise removal algorithms. *Journal of Physics D*, 60:259–268, 1992.

- [25] Yibin Tang, Yimei Xue, Ying Chen, and Lin Zhou. Blind deblurring with sparse representation via external patch priors. *Digit. Signal Process.*, 78:322–331, 2018.
- [26] A. B. Taylor. *Convex interpolation and performance estimation of first-order methods for convex optimization*. PhD thesis, Catholic University of Louvain, Louvain-la-Neuve, Belgium, 2017.
- [27] Robert Tibshirani. Regression shrinkage and selection via the lasso. *J. R. Stat. Soc. Series B Stat. Methodol.*, 58(1):267–288, 1996.
- [28] Rui Wang, Chunjie Zhang, Xiaolong Zheng, Yisheng Lv, and Yao Zhao. Joint defocus deblurring and superresolution learning network for autonomous driving. *IEEE Intell. Transp. Syst. Mag.*, 16(1):104–115, 2024.
- [29] Yangguang Wang, Chenxu Jiang, Xu Jia, Yufei Guo, and Lei Yu. Event-based shutter unrolling and motion deblurring in dynamic scenes. *IEEE Signal Process. Lett.*, 31:1069–1073, 2024.
- [30] Zhi Wang, Jianjun Wang, Wendong Wang, Chao Gao, and Siqi Chen. A novel thresholding algorithm for image deblurring beyond nesterov’s rule. *IEEE Access*, 6:58119–58131, 2018.
- [31] Zhou Wang, Alan C. Bovik, Hamid R. Sheikh, and Eero P. Simoncelli. Image quality assessment: from error visibility to structural similarity. *IEEE Trans. Image Process.*, 13(4):600–612, 2004.
- [32] Xu Yang, Wenquan Feng, Chen Zhuang, Qiang Wang, Xu Yang, and Zhe Yang. A multi-correlation peak phase deblurring algorithm for beidou B1C signals in urban environments. *Remote. Sens.*, 15(17):4300, 2023.
- [33] Hao Zhang, Te Qi, and Tiejong Zeng. Quaternion-aware low-rank prior for blind color image deblurring. *J. Sci. Comput.*, 101(2):27, 2024.
- [34] Hong Zhang, Yujie Wu, Lei Zhang, Zeyu Zhang, and Yawei Li. Image deblurring using tri-segment intensity prior. *Neurocomputing*, 398:265–279, 2020.
- [35] Jingwen Zhang, Xiaoxuan Zhou, Liyuan Li, Tingliang Hu, and Fansheng Chen. A combined stripe noise removal and deblurring recovering method for thermal infrared remote sensing images. *IEEE Trans. Geosci. Remote. Sens.*, 60:1–14, 2022.
- [36] Pei Zhang, Haosen Liu, Zhou Ge, Chutian Wang, and Edmund Y. Lam. Neuromorphic imaging with joint image deblurring and event denoising. *IEEE Trans. Image Process.*, 33:2318–2333, 2024.